Phase Equilibria for the Mean-Force Potential of Globular Protein Solutions

Frederico W. Tavares and Stanley I. Sandler
Center for Molecular and Engineering Thermodynamics, Dept. of Chemical Engineering, University of Delaware, Newark, DE 19716

When polymers are added to a solution containing proteins, the protein may deposit as an amorphous precipitate or as crystals. Experimental evidence indicates that from a thermodynamic viewpoint, an amorphous precipitate should be treated as a liquid phase dense in the protein and crystals as true solids. To understand the conditions under which protein precipitation or crystallization may occur, Gibbs-ensemble Monte Carlo simulation and Gibbs–Duhem integration techniques are used to calculate the liquid–liquid and liquid–solid phase boundaries for protein precipitation induced by polymers. In these simulations, the system is modeled using the pseudo-one-component approximation with an appropriate potential of mean force. The critical point for fluid–fluid phase equilibrium disappears as the attractive part of the mean-force potential becomes very short ranged. The accuracy of the second-order Barker and Henderson perturbation theory is examined by comparing the phase diagram predicted using this method with the simulation results. Perturbation theory is able to predict the general trends observed in the simulations but not with quantitative accuracy. Perturbation theory is then used to examine a broader range of conditions for protein deposition.

Introduction

Phase separation induced by the addition of a nonadsorbing polymer is important in the purification of globular proteins in the pharmaceutical, food, alcoholic beverage, and related industries, and of colloids in the paper, cosmetic, and soaps industries. This separation technique, normally carried out at ambient temperatures, is considered gentle enough to separate sensitive proteins, and it is relatively easy to scale up the process. These advantages make this separation/purification process useful for industrial purposes.

An increasing number of experimental studies (Vrij, 1976; de Hek and Vrij, 1981; Vincent et al., 1980; Sperry et al., 1981; Haire et al., 1984; Forciniti et al., 1991) have provided descriptions of the aqueous phase separation of colloids and proteins induced by polymers. Experimentally two major effects in the polymer-induced phase separation of the aqueous globular protein systems are observed. First, large proteins precipitate at a lower concentration of polymer than small proteins, and the solubility of proteins decreases with increasing molecular weight of polymer. Second, as a result of electrochemical effects, protein solubility decreases as the pH of the solution approaches the isoelectric point of the protein, and protein solubility also decreases with increasing ionic strength of the solution. Another important observation is that under some conditions the protein precipitate is amorphous, while at other conditions crystals are formed.

Models have been published to describe the behavior of these complex systems by using the one-component mean-force potential approximation. For example, Verwey and Overbeek (1948), Asakura and Oosawa (1958), Vrij (1976), Joanny et al. (1979), de Hek and Vrij (1981), Gast et al. (1983,b), Grimson (1983), and Victor and Hansen (1984) have used the one-component mean-force approximation for modeling the interactions in the colloidal dispersions, whereas Mahadevan and Hall (1990, 1992), Vlachy and Prausnitz (1992), Vlachy et al. (1993) have used the model to describe aqueous globular proteins in solutions of low salt concentration, and Chiew et al. (1995) and Kuehner et al. (1995) used a similar approach for solutions of high salt concentration.

Modeling a protein or colloid solution with a properly chosen potential of mean force should lead to a satisfactory description of the phase behavior; the thermodynamic proper-

Correspondence concerning this article should be addressed to S. I. Sandler.
Permanent address of F. W. Tavares: Escola de Química (DEQ), Universidade Federal do Rio de Janeiro, CP: 68542, CEP: 21949-970, Rio de Janeiro, Brazil.

ties and phase-separation conditions of protein solutions described by such models have been computed using a number of different statistical-mechanical approximation methods. These methods can be characterized as based on the osmotic virial expansion (Edmond and Ogston, 1968; Vilker et al., 1981; Haynes et al., 1992), statistical-mechanical perturbation theory (Gast et al., 1983a,b; Lekkerkerker et al., 1992; Mahadevan and Hall, 1990, 1992), integral-equation theory (Haynes et al., 1993), or the random-phase approximation (Grimson, 1983; Vlachy et al., 1993; Chiew et al., 1995; Kuehner et al., 1995).

By using the second-order Baker and Henderson perturbation theory with the Asakura and Oosawa (1954, 1958) osmotic attraction as the dominant contribution to the mean-force potential, Gast et al. (1983a,b) and Mahadevan and Hall (1990) have studied the polymer-induced phase separations of aqueous and nonaqueous colloidal and nonadsorbed protein systems. For the polymer sizes for which data have been reported, predictions based on this method led to a solid-fluid phase transition rather than the fluid-fluid phase separation observed experimentally by de Hek and Vrij (1981) for colloidal systems. However, Gast et al. (1983a) have shown that perturbation theory together with the Asakura-Oosawa potential can predict both fluid-fluid and solid-fluid transitions when very large polymer molecules are present. Nevertheless, statistical-mechanical perturbation theory is able to predict the experimentally observed dependencies on protein size, polymer size, protein concentration, and electrolyte concentration. As pointed out by Vlachy et al. (1993), the major disadvantage of perturbation theory is its complexity, which requires substantial numerical effort to calculate the complete phase diagram. However, as we find here, a considerable reduction in the numerical effort can be achieved by using the analytic radial distribution function for hard spheres recently published by Chang and Sandler (1994a).

Based on the experimental studies of de Hek and Vrij (1981) for colloidal systems and of Shih et al. (1992) for protein solutions, which suggest that polymer- (or salt-) induced protein (or colloid) precipitation may be more appropriately viewed as phase separation resulting in two fluid phases, Grimson (1983), Vlachy et al. (1993), Chiew et al. (1995), and Kuehner et al. (1995) have used the random-phase approximation to predict a fluid-fluid phase separation for a similar mean-force potential to that used in the perturbation theory calculations mentioned earlier. The major advantage of the random-phase approximation is its simplicity; little computational effort is required to calculate the whole phase diagram. The random-phase approximation has been used to qualitatively predict the general size and electrochemical effects observed in experiment.

The recent strategy in developing phase-equilibrium models is to combine intermolecular potential information with statistical thermodynamic approximations necessary to obtain an analytic expression. To establish rational engineering models for protein solutions, it is important to employ adequate statistical-mechanical approximations, with whatever one-component potential of mean-force model is used. Molecular simulation methods have become increasingly important in the development and testing of thermodynamic models, and can be considered an intermediate between direct experimental measurements and engineering models (Panagiotopoulos, 1994). Hagen and Frenkel (1994) have computed the phase diagram for the hard-core attractive Yukawa fluid using Monte Carlo simulation. From the results of Gibbs-ensemble simulations and Gibbs-Duhem integration, the authors have shown that the vapor-liquid coexistence curve disappears when a very short-range attraction potential is considered. When the range of the attractive part of the Yukawa potential is larger than approximately one-sixth of the hard-core diameter, the system can exist as a vapor, liquid, or solid, depending on the conditions, and both vapor-liquid and solid-liquid coexistence curves are possible. For shorter range interactions, the vapor-liquid critical point disappears and only the solid-fluid coexistence curve is thermodynamically stable. As Hagen and Frenkel point out, the short-range nature of the Asakura and Oosawa (1954, 1958) potential suggests that similar behavior may occur in polymer-induced colloid (or protein) precipitation, especially when using a polymer of small relative size.

In this work we have used the Gibbs-ensemble Monte Carlo simulation method of Panagiotopoulos (1987) and the Gibbs-Duhem integration of Kofke (1993a,b) and Agrawal and Kofke (1995a,b) to calculate the fluid-fluid and fluid-solid phase diagrams for solutions of globular proteins with a specified potential of mean force. We have also investigated the accuracy of the second-order Barker and Henderson perturbation theory for this system by comparing the phase diagram predicted from perturbation theory with the simulation data. The perturbation theory used here is similar to that of Gast et al. (1983a,b) and Mahadevan and Hall (1990). The differences are that we have used the analytic radial distribution function of Chang and Sandler (1994a) to speed up the phase-equilibria calculations, and the local compressibility approximation to better account for the second-order term in the Barker and Henderson perturbation theory. Also, from simulations and perturbation theory calculations, we have determined how the critical point for fluid-fluid phase-equilibria changes and even disappears for some values of the mean-force potential parameters, and how this is related to the range of the attraction part of the potential.

Interaction Potential in Protein Solutions

Thermodynamic models based on the one-component potential of mean-force model have frequently been used to describe interactions in colloidal dispersion and protein solutions. At this time a complete multicomponent protein-aqueous solution model is too complex to be used in simulation and perturbation theory calculations. However, the experimental observations for these systems can be explained by using a simple one-component model with an appropriately chosen potential of mean force. In this model the parameters of the effective protein-protein potential are dependent on the solvent properties and on the concentrations of the polymers and electrolytes. Following Gast et al. (1983a,b), Mahadevan and Hall (1990), Vlachy et al. (1993), and Coen et al. (1995), the mean force protein-protein potential $u^*(r) = u(r)/k_BT^0$ contains a hard-sphere part plus a sum of three terms, which is given by

$$u^* = u_R^*(r) + u_A^*(r) + u_{OA}^*(r) \qquad r > d_2$$
$$u^* = \infty \qquad r < d_2, \qquad (1)$$

where d_2 is the effective hard sphere diameter of the protein; $u_R^*(r) = u_R(r)/k_BT^0$ is the screened Coulomb repulsive interaction, $u_A^*(r) = u_A(r)/k_BT^0$ is the attractive van der Waals term, and $u_{OA}^*(r) = u_{OA}/k_BT^0$ is the potential due to the osmotic attraction proposed by Asakura and Oosawa (1954, 1958). Here k_B and T^0 are the Boltzmann constant and a convenient reference temperature (for example, $T^0 = 298$ K), respectively. In order to obtain more general results from the Gibbs-ensemble simulations, the Gibbs–Duhem integration, and perturbation theory, the potential contributions will be written in terms of nondimensional parameters as follows:

(a) Screened Coulomb repulsive contribution:

$$u_R^* = \frac{A^*}{s(1+k^*/2)^2}\exp[-k^*(s-1)] \qquad s>1 \qquad (2)$$

and

$$A^* = \frac{(z_2e)^2}{4\pi\epsilon_0\epsilon_R k_B T^0 d_2} \qquad (3)$$

$$k^* = kd_2 = \left(\frac{2e^2Id_2^2N_A}{\epsilon_0\epsilon_R k_B T^0 T^*}\right)^{1/2}. \qquad (4)$$

In these expressions, $s = r/d_2$ is the relative distance between macroion centers; z_2e is the charge on a polyion (this quantity is related to the pH of the solution and is a unique function for each protein); ϵ_R is the relative permitivity of the solution; k^{-1} is the Debye screening length which is directly related to the ionic strength $I = 1/2\ \Sigma z_i^2 n_i$ of the solution; N_A is Avogadro's number; and $T^* = T/T^0$ is the reduced temperature of the system.

(b) Attractive van der Waals term:

$$u_A^* = -\frac{H^*}{36}(1/s)^6 \qquad s>1, \qquad (5)$$

where $H^* = H/k_BT^0$ and H is the Hamaker constant.

(c) Attractive osmotic potential of Asakura and Oosawa (1954, 1958):

$$u_{OA}^* = -\frac{4\pi d_3^3\rho_3^*T^*}{3d_3^{*3}}\left(1-\frac{3s}{4d}+\frac{s^3}{16d^3}\right) \qquad 1<s<2d \qquad (6)$$

$$u_{OA}^* = 0 \qquad s>2d, \qquad (7)$$

where $d_3^* = d_3/d_2$ with d_3 being the diameter of the polymer; $2d = (d_2+d_3)/d_2$ is the maximum relative distance at which the osmotic forces are important; and $\rho_3^* = d_3\rho_3$ is the reduced density of the polymer. For simplicity, we have used the ideal osmotic pressure approximation; a better approximation can be obtained by incorporating information for the second virial coefficient that accounts for polymer–polymer interactions (Gast et al., 1983b). The general shape and short-range character of the Asakura and Oosawa potential are shown in Figure 1a. For a fixed volumetric concentration of polymer ρ_3^*, the short-range nature of this potential becomes more pronounced as the relative diameter d_3/d_2 decreases.

The parameters A^*, k^*, H^*, ρ_3^*, and d_3/d_2 have to be specified *a priori* and, in general, these parameters depend upon the sizes of polymer and protein, the concentration of polymer and salt, the electrochemical characteristics of the protein, and on the other properties of the solution (e.g., pH, T^*, I, and ϵ_R). We have calculated these values for the conditions used by Vilker et al. (1981), Mahadevan and Hall (1990), and Vlachy et al. (1993). The range of these parameters is $A^* = 0$ to 20; $k^* = 1.5$ to 20; $H^* = 2$ to 10; $\rho_3^* = 0.05$ to 1.5; and $d_3/d_2 = 0.04$ to 0.5. Figures 1b, 1c and 1d show each contribution and the overall potential for different values of these parameters. From these figures we see that for the conditions reported the volume-exclusion (osmotic) potential is the dominant part of the overall potential, and the short-range attraction is almost unaffected by changes in the solution properties. In some circumstances, as shown in Figure 1b, the screened Coulomb repulsive part effectively cancels out the attractive van der Waals contribution. Gast et al. (1983a,b) and Mahadevan and Hall (1990) have also pointed out that the Asakura and Oosawa (1954, 1958) osmotic attraction is the principal contribution to the potential of mean force for the prediction of the nonadsorbed polymer-induced phase separation of colloidal and protein solutions. For this reason in this article we mainly consider this contribution to the potential.

Simulation Techniques

In this section we briefly describe the simulation techniques used to map the phase diagrams of the Asakura and Oosawa fluid, Eqs. 6 and 7, for different values of the ratio d_3/d_2. This is the potential normally used to describe the destabilization or flocculation of nonaqueous colloidal suspensions by a nonadsorbing polymer, and it is also thought to be dominant for protein precipitation induced by a nonadsorbing polymer. Here, we combine the Gibbs-ensemble Monte Carlo simulation of Panagiotopoulos (1987) to calculate the fluid–fluid phase transition with the Gibbs–Duhem integration of Kofke (1993a,b) and Agrawal and Kofke (1995a,b) to calculate the solid–fluid equilibrium phase coexistence in order to determine the complete phase diagram of the fluid.

Gibbs-ensemble Monte Carlo simulation

Gibbs-ensemble Monte Carlo simulation (Panagiotopoulos, 1987; Panagiotopoulos et al., 1988) is the standard method for calculating fluid–fluid phase equilibria. This method has been applied to many different potential models and physical situations; extensive reviews have been published elsewhere (Panagiotopoulos, 1992, 1994).

In the context of the one-component potential of mean-force approximation we are using, the Gibbs-ensemble simulation predicts a phase separation similar to the vapor–liquid equilibria transition, but here corresponding to the coexistence of liquid solutions of low and high concentrations of protein, respectively. The method is based on performing a Monte Carlo simulation in two distinct boxes that represent the two coexisting macroscopic phases. In order to avoid interface problems, conventional boundary conditions (Allen

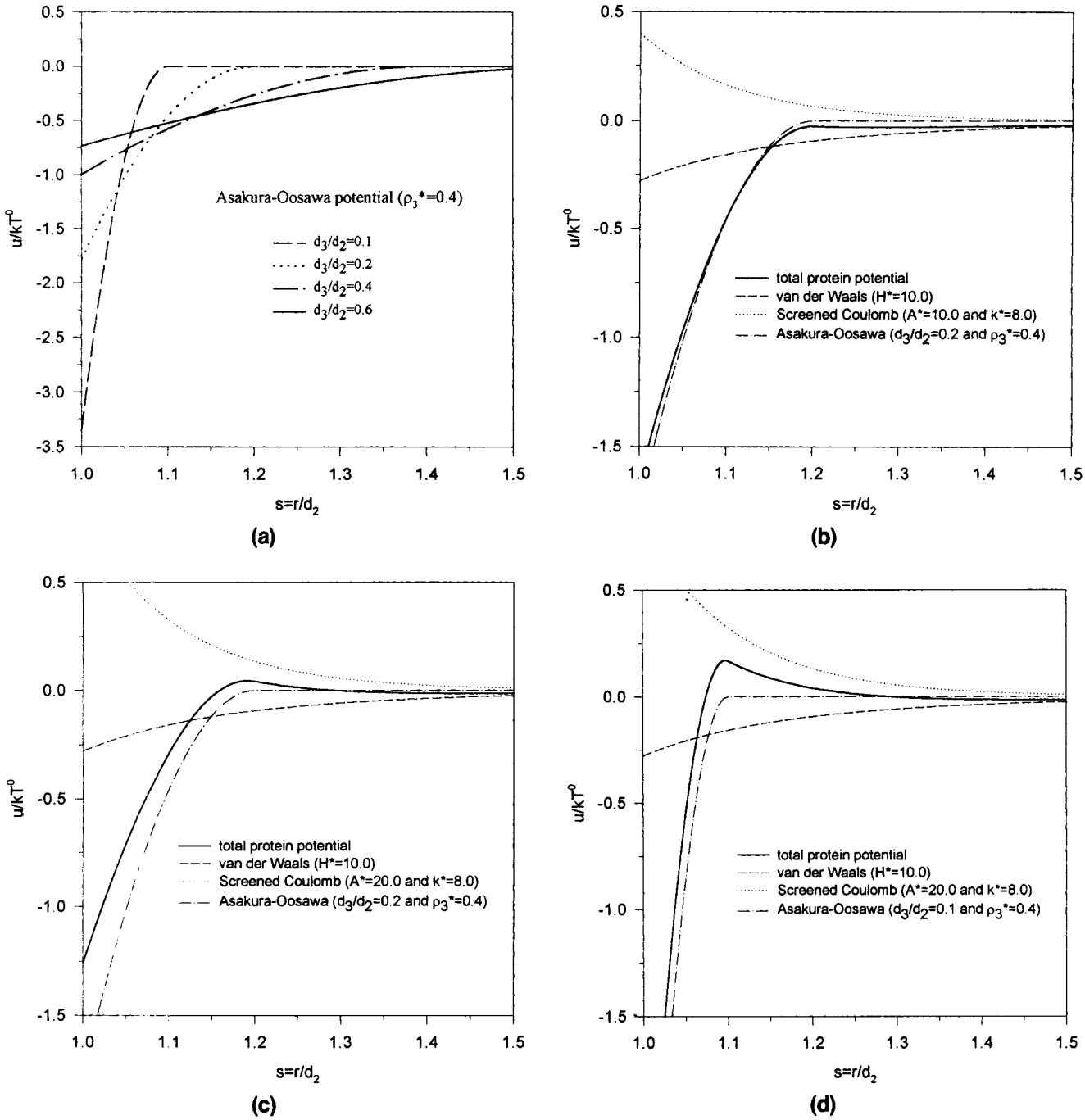

Figure 1. Asakura and Oosawa potential (a) and the total protein potential (b, c, and d).

and Tildesley, 1987) are imposed in all directions for each box. Internal displacements, volume changes, and particle transfers are performed in a way that ensures that the thermodynamic equilibrium conditions for phase coexistence are statistically satisfied. Since details of the Gibbs-ensemble simulation technique can be found in other references (Panagiotopoulos, 1987; Panagiotopoulos et al., 1988; Smit, 1990; Smith and Frenkel, 1991b), these are not discussed here.

All the simulations were carried out with 300 particles and started from a face-centered cubic-lattice initial configuration, and therefore require a number of cycles to relax to an equilibrium condition. After at least 5,000 cycles for equilibration, the phase coexistence and thermodynamic properties were calculated over another 10,000 cycles. The maximum displacement and the maximum attempted volume change were adjusted to give acceptance ratios of between 40 and 50%; the attempted interchanges per cycle were equal to the total number of particles. Table 1 gives the results from the Gibbs ensemble simulation of the Asakura and Oosawa potential for the case of very large polymer, $d_3/d_2 = 1.0$. In this table, ρ_3^* is the reduced polymer density, and $\rho_2^{*V} = d_2^3 \rho_2^V$ and $\rho_2^{*L} = d_2^3 \rho_2^L$ are the reduced "vapor" and "liquid" densities of protein, respectively. The numbers in parentheses refer to the standard deviation of the thermodynamic proper-

Table 1. Vapor-Liquid Coexistence Thermodynamic Properties for the Asakura-Oosawa Potential for $d_3/d_2 = 1.0$, Obtained from the Gibbs Ensemble Simulation

$1/\rho_3^*$	ρ_3^*	ρ_2^{*V}	ρ_2^{*L}
1.0638	0.94	0.097(11)	0.568(10)
1.0526	0.95	0.0867(36)	0.577(15)
1.0417	0.96	0.0751(36)	0.589(12)
1.0204	0.98	0.0611(11)	0.615(11)
1.0101	0.99	0.0520(12)	0.622(15)
0.9091	1.10	0.0256(8)	0.731(14)
0.8333	1.20	0.0161(3)	0.801(9)

ties estimated from subaverages over 1,000 cycles. The relative uncertainty of the simulation, directly related to the standard deviation, increases on approaching the critical point. It is pointed out by Recht and Panagiotopoulos (1993), the vapor–liquid phase behavior of pure three-dimensional Lennard-Jones fluid does not exhibit a strong finite-size effect; we expect the same behavior with the Asakura–Oosawa potential, so that our 300-particle simulations should be satisfactory.

As pointed out by Gast et al. (1983a) and Vlachy et al. (1993), for the Asakura and Oosawa potential with the ideal osmotic pressure, the parameter $(1/\rho_3^*)$ plays a similar role to the reduced temperature for the simple potentials considered here. We have used this observation to determine the critical point with respect to polymer concentration of the Asakura and Oosawa fluid for a polymer relative diameter of $d_3/d_2 = 1.0$. The critical reduced polymer density (ρ_3^{*C}) and the critical reduced protein density (ρ_2^{*C}) were estimated by correlating the protein densities in the dilute and concentrated phases obtained from the Gibbs-ensemble Monte Carlo simulations with the classic scaling expressions (Yeomans, 1992),

$$\rho_2^{*L} - \rho_2^{*V} = B(1/\rho_3^{*C} - 1/\rho_3^*)^{\beta} \tag{8}$$

$$\frac{\rho_2^{*L} + \rho_2^{*V}}{2} = \rho_2^{*C} + A(1/\rho_3^{*C} - 1/\rho_3^*)^{\delta}, \tag{9}$$

where the 3-D–Ising model scaling parameters ($\beta = 0.326$ and $\delta = 0.875$) were used in the fitting procedure. The parameters A and B, and the critical polymer and protein densities were determined using a nonweighted least squares method. Figure 2 shows the good agreement obtained with this fitting procedure; the critical polymer and protein densities were found to be $\rho_2^{*C} = 0.298 \pm 0.008$ and $(1/\rho_3^{*C}) = 1.123 \pm 0.004$ with this procedure.

Gibbs – Duhem integration

We have used the Gibbs–Duhem integration technique developed by Kofke (1993a,b) and Agrawal and Kofke (1995a,b) to calculate the crystalline solid–fluid coexistence properties. The method is based on the direct integration of the Clausius–Clapeyron equation

$$\frac{dP}{d\beta} = -\frac{\Delta h}{\beta \Delta v}, \tag{10}$$

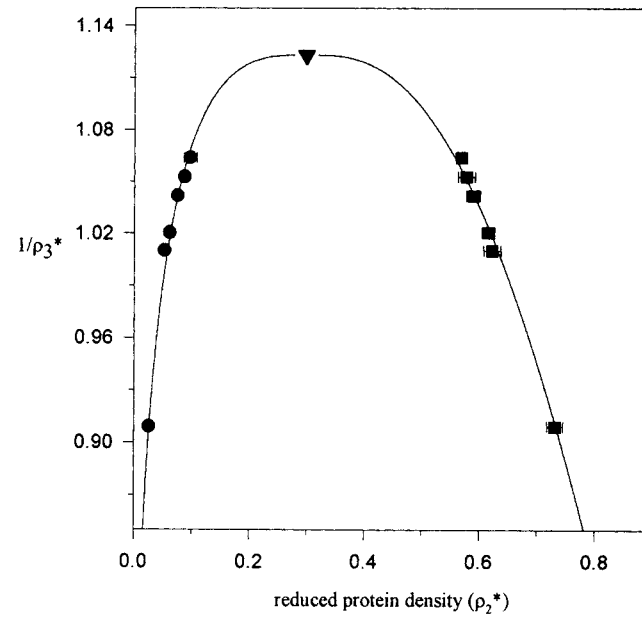

Figure 2. Vapor–liquid coexistence curve for the Asakura and Oosawa potential with $d_3/d_2 = 1.0$.

The circles are the vapor and the squares are the liquid densities obtained form the Gibbs-ensemble Monte Carlo simulation. The line is the fit to the scaling law, and the triangle is the critical point estimated from this fitting procedure.

where $\beta = 1/k_B T$, P is the pressure, and $\Delta h = h_F - h_S$ and $\Delta v = v_F - v_S$ are the differences in molar enthalpies and volumes between the fluid and solid phases, respectively. To map the melting curve, it is more convenient to rewrite the Clausius–Clapeyron equation in terms of energy differences, instead of enthalpies, and in terms of nondimensional variables as follows:

$$\frac{d\ln(\beta^* P^*)}{d\beta^*} = -\frac{\Delta e^*}{\beta^* P^* \Delta v^*} = f(\beta^*, P^*). \tag{11}$$

The reduced variables are $\beta^* = \epsilon/k_B T$, $P^* = P\sigma^3/\epsilon$, $v^* = v/\sigma^3$, and $e^* = e/\epsilon = (h - Pv)/\epsilon$ is the reduced energy, where e is the configurational internal energy and ϵ and σ are, respectively, the characteristic energy and diameter parameters. Equation 11 is a first-order nonlinear equation, and it defines how the pressure must change with temperature (here polymer density) for the two phases to remain in thermodynamic equilibrium. With a knowledge of an initial condition, this equation can be integrated numerically to compute the coexistence points, with $f(\beta^*, P^*)$ evaluated using an NPT-ensemble Monte Carlo or molecular dynamics simulation applied independently to each phase for a specified condition of β^* and P^*. The proper integration of this expression automatically ensures the equality of the chemical potentials in both phases, and since no particle insertions are needed, this approach can be used for the determination of the solid–fluid coexistence line, a case for which the Gibbs-ensemble technique cannot be easily used.

Our use of the Kofke integration scheme with the Asakura and Oosawa potential is based on the direct integration of

the preceding Clausius–Clapeyron equation by making the following identification of the potential parameters $\epsilon = \rho_3^* k_B T$ and $\sigma = d_2$. Thus Eq. 11 can be rewritten as

$$\frac{d \ln(\rho_3^* P^*)}{d\rho_3^*} = -\frac{\Delta e^*}{\rho_3^* P^* \Delta v^*} = f(\rho_3^*, P^*). \qquad (12)$$

The differences in molar energies and volumes between the fluid and crystalline solid phases, and consequently $f(\rho_3^*, P^*)$, were evaluated using NPT-ensemble Monte Carlo simulations. In order to integrate this equation, a fourth-order predictor–corrector algorithm was used as proposed by Kofke. To initiate this procedure, the pressure and densities of the coexisting phases of the hard-sphere fluid at melting of Hoover and Ree (1968) were used as an initial condition at the limit $\rho_3^* \to 0$ ($\rho_3^* P^* = 11.69$, $\rho_2^{*F} = 0.943$, and $\rho_2^{*S} = 1.041$). The initial slope, the righthand side of the Eq. 12, has a finite limit and was calculated using canonical-ensemble Monte Carlo simulations for each phase. In particular, simulation of 108-particle hard-sphere-FCC crystal and 100-particle hard-sphere fluid were used to evaluate the reduced configurational energy of the Asakura–Oosawa attractive potential in both phases. Values of $f(\rho_3^* \to 0, \rho_3^* P^* = 11.69)$ were obtained as mean values of at least two simulations over 10,000 equilibration and 30,000 production cycles. The subsequent values of $f(\rho_3^*, P^*)$ were obtained from NPT-ensemble Monte Carlo simulations. These simulations were carried out using 108 and 100 particles in the solid and fluid phases, respectively. The results presented here were obtained from simulations over 9,000 cycles for equilibration followed by 9,000 production cycles for each NPT-ensemble set. The maximum trial displacement of a particle and volume changes were adjusted such that the acceptance of trial moves varied between 35 and 50%. Standard cubic periodic boundary conditions and the minimum image convention were used in both phases. The cubic FCC-crystal structure was assumed for the solid phase, as suggested and justified by Hagen and Frenkel (1994). Also, the Hoover one-occupancy model (corresponding, for the cubic FCC-crystal structure, to the rhombododecahedra Wigner–Seitz cell) was used to avoid a possible nonexpected melting of the solid phase.

At the beginning of the integration procedure (i.e., for values of ρ_3^* close to zero), the function $f(\rho_3^*, P^*)$ has a small and approximately constant value. In this region, the integration can be carried out without using very small integration steps ($\Delta\rho_3^*$). However, in the region where the function $f(\rho_3^*, P^*)$ or its derivative with respect to ρ_3^* is large in magnitude, a small integration step is needed to obtain reasonable values for the thermodynamic properties. One criterion used to reject the integration results in a given region and to restart the integration with a smaller value of $\Delta\rho_3^*$ was based on the comparison at each step of the pressure obtained from the integration procedure and the pressure calculated using the virial equation (Smit and Frenkel, 1991a) in the NPT-ensemble simulation of the fluid phase. It should be clear that this criterion provides only a measure of the convergence of the NPT-ensemble simulations, and it is not a direct measure of the accuracy of the integration procedure. The size of the step $\Delta\rho_3^*$ was found to be related to the short-range behavior of the potential; smaller values of d_3/d_2 require smaller step sizes $\Delta\rho_3^*$.

Table 2. Solid-Fluid Coexistence Thermodynamic Properties for the Asakura-Oosawa Potential for $d_3/d_2 = 1.00$, Obtained from Gibbs-Duhem Integration

ρ_3^*	ρ_2^{*F}	ρ_2^{*S}
0.05	0.963(1)	1.052(9)
0.10	0.932(6)	1.058(9)
0.15	0.928(3)	1.047(11)
0.20	0.942(4)	1.036(14)
0.25	0.936(8)	1.066(12)
0.30	0.947(8)	1.038(8)
0.35	0.955(4)	1.052(2)
0.40	0.949(12)	1.052(4)
0.45	0.931(5)	1.063(6)
0.50	0.944(7)	1.076(12)
0.55	0.946(5)	1.048(4)
0.60	0.944(5)	1.038(8)
0.65	0.945(9)	1.078(10)
0.70	0.949(8)	1.087(11)
0.75	0.942(7)	1.082(7)
0.80	0.930(4)	1.072(7)
0.85	0.949(5)	1.077(10)
0.90	0.935(3)	1.086(1)
0.95	0.930(5)	1.071(2)
1.00	0.932(2)	1.073(5)
1.05	0.937(3)	1.085(4)
1.10	0.907(4)	1.053(6)
1.15	0.912(5)	1.065(3)
1.20	0.930(4)	1.077(7)

Tables 2, 3 and 4 summarize the results obtained from the Gibbs–Duhem integration technique using the Asakura and Oosawa potential for values of the relative polymer diameter (d_3/d_2) of 1.0, 0.20 and 0.14. In these tables, ρ_3^* is the reduced polymer density, and $\rho_2^{*S} = d_2^3 \rho_2^S$ and $\rho_2^{*F} = d_2^3 \rho_2^F$ are the reduced solid and fluid protein densities, respectively. Again, the numbers in parentheses refer to the standard deviation of the thermodynamic properties estimated from subaverages over 3,000 cycles.

Perturbation Theory

In this section the Helmholtz free energy and the equation of state used to predict the phase diagram for the one-component mean-force potential model are obtained using second-order Barker and Henderson perturbation theory. Calculations for both the full potential containing contributions from the charge–charge interaction, the van der Waals attraction and the volume-exclusion effect, and for only the Asakura–Oosawa potential are presented. In perturbation theory, the Helmholtz free energy of the system is expanded around that of a reference system whose thermodynamic properties and structural information are well known. As pointed out by Boublik et al. (1980), the second-order Baker and Henderson perturbation theory with the local compressibility approximation is more accurate in predicting the properties of the Lennard-Jones fluid than the same calculations with the macroscopic compressibility approximation. Using the local compressibility approximation for the second-order contribution, the Helmholtz free energy from Barker and Henderson perturbation theory, for a potential written as $u = u_0 + u_p$, is (McQuarrie, 1976)

Table 3. Solid-Fluid Coexistence Thermodynamic Properties for the Asakura-Oosawa Potential for $d_3/d_2 = 0.20$, Obtained from the Gibbs Integration

ρ_3^*	ρ_2^{*F}	ρ_2^{*S}
0.04	0.946(5)	1.072(7)
0.08	0.949(4)	1.087(4)
0.12	0.949(10)	1.113(4)
0.16	0.943(2)	1.137(4)
0.20	0.960(7)	1.131(2)
0.240	0.952(6)	1.163(2)
0.280	0.948(2)	1.200(6)
0.320	0.934(3)	1.220(4)
0.360	0.902(4)	1.250(2)
0.400	0.896(3)	1.270(6)
0.410	0.872(10)	1.280(1)
0.420	0.855(2)	1.284(1)
0.430	0.852(1)	1.284(1)
0.440	0.840(4)	1.284(1)
0.450	0.853(8)	1.283(1)
0.460	0.834(5)	1.283(1)
0.470	0.794(7)	1.282(1)
0.480	0.772(7)	1.282(1)
0.485	0.758(2)	1.300(2)
0.490	0.739(1)	1.302(3)
0.495	0.688(5)	1.304(2)
0.500	0.645(8)	1.301(3)
0.505	0.609(6)	1.304(3)
0.510	0.564(6)	1.290(3)
0.515	0.528(7)	1.300(4)
0.520	0.339(1)	1.300(4)
0.525	0.254(20)	1.295(4)
0.530	0.132(13)	1.308(2)
0.535	0.033(2)	1.310(3)
0.540	0.032(1)	1.312(1)
0.545	0.027(2)	1.309(2)
0.550	0.025(2)	1.313(1)
0.555	0.023(2)	1.308(3)
0.560	0.020(1)	1.321(2)
0.565	0.017(1)	1.315(1)
0.570	0.016(4)	1.315(2)
0.575	0.015(1)	1.318(2)
0.580	0.013(2)	1.320(3)
0.585	0.012(2)	1.316(2)
0.590	0.011(2)	1.322(2)
0.595	9.6(1)e-3	1.322(2)
0.600	8.6(1)e-3	1.321(2)
0.605	7.6(1)e-3	1.327(1)
0.610	7.0(2)e-3	1.325(2)
0.615	6.14(1)e-3	1.329(3)
0.620	5.45(2)e-3	1.322(1)
0.625	4.90(4)e-3	1.328(4)

$$\frac{A}{Nk_BT} = \frac{A_0}{Nk_BT} + \frac{2\pi\rho}{k_BT}\int_{d_2}^{\infty} u_p g_0 r^2\, dr - \frac{\pi\rho}{(k_BT)^2}\int_{d_2}^{\infty} (u_p)^2 k_BT \left(\frac{\partial(\rho g_0)}{\partial P}\right)_0 r^2\, dr, \quad (13)$$

where A and A_0 are the Helmholtz free energies of the protein at the same number density and temperature for the complete potential and the reference potential, respectively, N is the number of molecules, k_B is the Boltzmann constant, T is the temperature, u_0 is the hard-sphere reference potential, u_p is the perturbation potential, and g_0 is the radial distribution function for the reference system (hard-sphere

Table 4. Solid-Fluid Coexistence Thermodynamic Properties for the Asakura-Oosawa Potential for $d_3/d_2 = 0.14$, Obtained from the Gibbs Integration

ρ_3^*	ρ_2^{*F}	ρ_2^{*S}
0.020	0.950(4)	1.065(3)
0.040	0.953(4)	1.067(7)
0.060	0.963(4)	1.055(18)
0.080	0.977(11)	1.070(3)
0.100	0.973(5)	1.092(3)
0.140	0.984(2)	1.126(6)
0.160	0.985(4)	1.137(8)
0.180	0.997(3)	1.173(3)
0.200	0.971(12)	1.205(5)
0.210	0.993(3)	1.249(17)
0.220	1.000(2)	1.303(2)
0.230	0.988(3)	1.316(7)
0.240	0.978(1)	1.315(2)
0.250	0.952(3)	1.308(2)
0.260	0.954(2)	1.318(1)
0.270	0.947(1)	1.316(4)
0.280	0.934(2)	1.322(1)
0.290	0.917(3)	1.324(4)
0.300	0.879(3)	1.321(1)
0.310	0.873(3)	1.327(3)
0.320	0.855(3)	1.328(2)
0.330	0.850(5)	1.323(1)
0.340	0.818(1)	1.330(2)
0.350	0.786(6)	1.337(2)
0.360	0.744(3)	1.335(2)
0.370	0.722(7)	1.333(1)
0.380	0.699(5)	1.338(2)
0.382	0.650(2)	1.343(1)
0.384	0.647(3)	1.340(2)
0.386	0.642(3)	1.344(1)
0.388	0.631(3)	1.342(3)
0.390	0.634(2)	1.345(1)
0.392	0.624(4)	1.344(2)
0.394	0.614(7)	1.344(2)
0.396	0.628(5)	1.338(1)
0.398	0.612(3)	1.344(1)
0.400	0.578(10)	1.348(2)
0.402	0.551(1)	1.344(3)
0.404	0.561(8)	1.340(1)
0.406	0.546(2)	1.346(2)
0.408	0.535(3)	1.344(2)
0.410	0.515(2)	1.342(2)
0.412	0.500(8)	1.349(2)
0.414	0.463(10)	1.348(2)
0.416	0.429(1)	1.352(1)
0.418	0.396(1)	1.352(1)
0.420	0.363(2)	1.349(5)
0.422	0.369(5)	1.350(1)
0.424	0.360(6)	1.345(1)
0.426	0.340(6)	1.348(1)
0.428	0.323(4)	1.348(1)
0.430	0.309(5)	1.343(2)
0.432	0.296(3)	1.350(2)
0.434	0.268(6)	1.349(3)
0.436	0.232(2)	1.352(1)
0.438	0.217(3)	1.351(2)
0.440	0.200(2)	1.351(1)
0.442	0.187(1)	1.352(2)
0.444	0.171(5)	1.352(3)
0.446	0.162(4)	1.351(3)
0.448	0.142(3)	1.353(1)

(Table 4 continued)

Table 4. Continued

ρ_3^*	ρ_2^{*F}	ρ_2^{*S}
0.450	0.117(5)	1.351(1)
0.452	0.084(4)	1.346(2)
0.454	0.072(5)	1.351(2)
0.456	0.056(1)	1.353(1)
0.458	0.040(2)	1.355(2)
0.460	0.043(2)	1.356(3)
0.462	0.044(3)	1.352(2)
0.464	0.037(1)	1.356(1)
0.466	0.033(1)	1.356(1)
0.468	0.034(2)	1.354(1)
0.470	0.034(2)	1.357(1)
0.472	0.029(3)	1.353(2)
0.474	0.029(1)	1.357(1)
0.476	0.028(1)	1.355(1)
0.478	0.026(2)	1.359(2)

fluid). The derivative term in the second integral refers to the reference fluid and is given by

$$\left(\frac{\partial(\rho g_0)}{\partial P}\right)_0 = \frac{1}{\left(\frac{\partial P}{\partial \rho}\right)_0}\left[g_0 + \rho\left(\frac{\partial g_0}{\partial \rho}\right)\right]. \tag{14}$$

By substituting this expression into the Helmholtz free energy given earlier and using the packing fraction of protein defined as $\eta = \pi\rho d_2^3/6$, Eq. 13 can be expressed as the following series in reduced temperature, $T^* = T/T^0$,

$$\frac{A}{Nk_BT} = \frac{A_0}{Nk_BT} + \frac{12\eta}{T^*}I_1 - \frac{1}{T^{*2}}\frac{6\eta}{\left(\frac{\partial(P/k_BT)}{\partial\rho}\right)_0}\{I_2 + \eta I_2'\}. \tag{15}$$

The corresponding equation of state, expressed in terms of the compressibility factor Z, is obtained by differentiating the Helmholtz free energy with respect to the packing fraction η, and is

$$Z = Z_0 + \frac{12\eta}{T^*}(I_1 + \eta I_1') - \frac{1}{T^{*2}}\frac{6\eta}{\left(\frac{\partial(P/k_BT)}{\partial\rho}\right)_0}\left\{(I_2 + 3\eta I_2' + \eta^2 I_2'') - (\eta I_2 + \eta^2 I_2')\frac{\partial}{\partial\eta}\ln\left(\frac{\partial(P/k_BT)}{\partial\rho}\right)_0\right\}, \tag{16}$$

where

$$I_1 = \int_1^{s_{\max}} u_p^* g_0 s^2\, ds \qquad I_1' = \int_1^{s_{\max}} (u_p^*)\left(\frac{\partial g_0}{\partial\eta}\right)s^2\, ds$$

$$I_2 = \int_1^{s_{\max}} (u_p^*)^2 g_0 s^2\, ds \qquad I_2' = \int_1^{s_{\max}} (u_p^*)^2\left(\frac{\partial g_0}{\partial\eta}\right)s^2\, ds$$

$$I_2'' = \int_1^{s_{\max}} (u_p^*)^2\left(\frac{\partial^2 g_0}{\partial\eta^2}\right)s^2\, ds. \tag{17}$$

The first- and second-order perturbation theory terms were calculated separately and their magnitudes compared in order to test the convergence of the expansion for a specified parameter region of the potential. This expansion is expected to be valid as long as the value of the second term is small in magnitude compared to the first term. The reference fluid contributions, A_0 and Z_0, were calculated using the Carnahan–Starling (1969) and Hall (1971) equations of state for the fluid phase and the FCC-crystal solid phase, respectively. We have used the Percus–Yevick compressibility equation for the fluid phase to evaluate the term $[\partial(P/k_BT)/\partial\rho]_0$ that appears in the second-order perturbation contribution, as originally suggested by Barker and Henderson (1967). This contribution could have been evaluated using the Carnahan–Starling equation of state, but the difference is small. The contribution of this term for the solid phase was also calculated using the Hall (1971) equation of state. The perturbation part of the effective protein–protein potential is given by $u_p/k_BT^0 = u_p^* = u_R^* + u_A^* + u_{OA}^*$, and accounts for the screened Coulomb repulsive contribution, u_R^* of Eqs. 2–4, the attractive van der Waals interaction, u_A^* of Eq. 5, and the Asakura and Oosawa osmotic attraction, u_{OA}^* of Eqs. 6 and 7.

Recently, Chang and Sandler (1994a) presented a nonimaginary, analytical radial distribution function (RDF) for the hard-sphere system based on a shell-by-shell solution of the Percus–Yevick differential equation. We have used this expression to evaluate the thermodynamic properties of the hard-sphere reference system in the fluid phase. The Kincaid and Weis (1977) RDF expression for the hard-sphere potential in the FCC-crystal structure was used for the solid phase. Both radial distribution functions are nonimaginary analytic functions; their analytical first- and second-order derivatives were also used to calculate the integrals I_1, I_1', I_2, I_2', and I_2'' that appear in the perturbation expansion earlier. These integrals were evaluated using the Romberg integration method (Press et al., 1992), where $s_{\max}$ represents the cutoff distance of the potential. Due to the short-range character of the potential used here, $s_{\max}$ was always equal to or smaller than 2.0. The approach presented here is not restricted to short-range potentials since the analytic expressions for the RDF of hard-sphere systems for both phases are valid to distances of $4d_2$ (or $s_{\max} = 4$); however, evaluation of the integrals and the phase-equilibrium calculations are more time-consuming for longer range potentials.

Other thermodynamic properties, such as the Gibbs free energy, can be obtained directly from the Helmholtz free energy and equation-of-state expressions. In order to calculate the phase behavior, it is necessary to define the Gibbs free energy of the reference state. For the case of fluid–fluid equilibria, we have used the ideal gas state at the system temperature. The phase envelope was obtained by applying the Maxwell equal-area rule and comparing the chemical potential of both phases to confirm the equilibrium state. This procedure is similar to that previously reported by Chang and Sandler; more details about these calculations and the expressions for the RDF and their first and second derivatives can be found in Chang and Sandler (1994a,b). For solid–fluid equilibrium calculations, we have used the equality of chemical potentials as the equilibrium state criterion, and the hard-sphere Gibbs free energy at the condition of the coex-

istence of the phases (Hoover and Ree, 1968) as a reference state for both phases. The algorithm for the solid–fluid equilibrium calculations is similar to that used by Gast et al. (1983a,b) and Mahadevan and Hall (1990).

Results

Combining the information obtained from Gibbs-ensemble simulation and Gibbs–Duhem integration techniques, the phase diagrams of the Asakura and Oosawa potential, given by Eqs. 6 and 7, were mapped for several values of the relative polymer diameter (d_3/d_2). As shown in Figure 1, this potential is very short range in reduced units when the polymer diameter is much smaller than the protein diameter. By comparing with simulation results, we also test the ability of the second-order perturbation theory to predict the shape of the phase diagram for polymer-induced protein precipitation using the Asakura and Oosawa potential. Then, using second-order perturbation theory, we have been able to examine changes in the shape of the phase diagram due to the charge–charge interaction and due to the van der Waals contribution, by adding the screened Coulomb repulsive expression of Eqs. 2–4, and the attractive van der Waals term of Eq. 5 in the perturbation potential.

Figure 3 presents the phase diagram of the Asakura and Oosawa potential for a very large polymer ($d_3/d_2 = 1.0$). As can be seen from this figure, the system has regions where the vapor, liquid, solid phase may exist as the stable phase, or two or more phases may coexist depending on the polymer and protein densities. In the context of the one-component mean-force potential model, these multiple phases mean that the system may exist as a dilute-protein phase, as a concentrated-protein amorphous-precipitate phase, and as a crystallized-protein phase, represented here by vapor, liquid, and solid phases, respectively. In the region of low protein densities, the symbols represent liquid–liquid coexistence conditions given by Gibbs-ensemble Monte Carlo simulations (which corresponds to vapor–liquid equilibrium in a true one-component fluid). The critical point, indicated by the triangle in the figure, was estimated using the law of rectilinear diameters and using the 3D-Ising exponent parameters in the scaling laws (Tavares and Sandler, 1996). In the region of high protein densities, the symbols represent the solid–fluid coexistence transition calculated using the Gibbs–Duhem integration technique. In Figure 3 the solid–fluid and vapor–liquid phase coexistence lines and the vapor–liquid critical point obtained from the second-order perturbation theory are shown. Perturbation theory leads to predictions of the same general behavior as observed from simulation. However, as expected, perturbation theory overpredicts the location of the critical point of the vapor–liquid transition in terms of $1/\rho_3^{*C}$. These results show that the solid–fluid coexistence is only stable for very high concentrations (densities) of protein, and the system has a triple point at a very high concentration of polymer (high density of polymer ρ_3^*).

Figures 4 and 5 present the phase diagrams of the Asakura and Oosawa potential for two other values of the relative polymer diameter, $d_3/d_2 = 0.20$ and 0.14, respectively. As shown in Figure 1a, the variation of the parameter d_3/d_2 from 1.0 to 0.14 results in a much shorter range (in reduced units) of the effective protein–protein potential. For both cases ($d_3/d_2 = 0.20$ and 0.14) the system has only a solid–fluid transition, which was obtained using Gibbs–Duhem integration and is shown in the figures with the square and circle

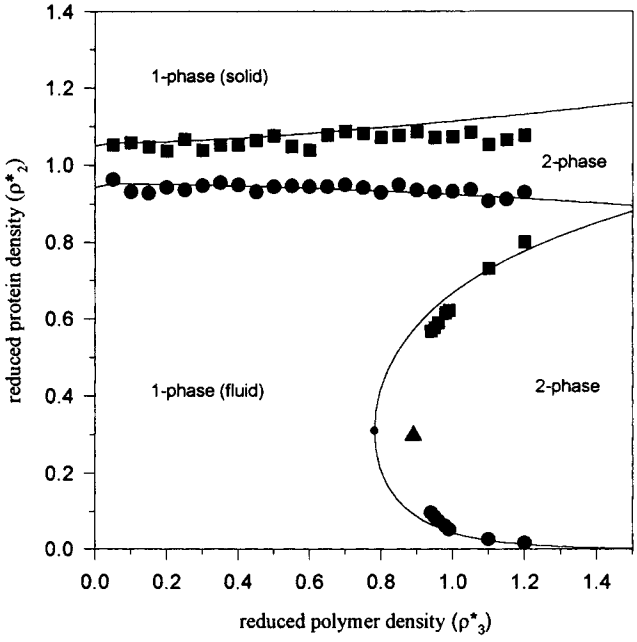

Figure 3. Phase diagram for the Asakura and Oosawa fluid for $d_3/d_2 = 1.0$.

Symbols are the Gibbs–Duhem integration (solid–fluid) and the Gibbs-ensemble simulation (vapor–liquid) results. The triangle is the critical point obtained from the fitting of the Gibbs-ensemble density points to the scaling law. The lines and the filled circles are the phase-equilibrium and critical-point results, respectively, obtained from second-order perturbation theory.

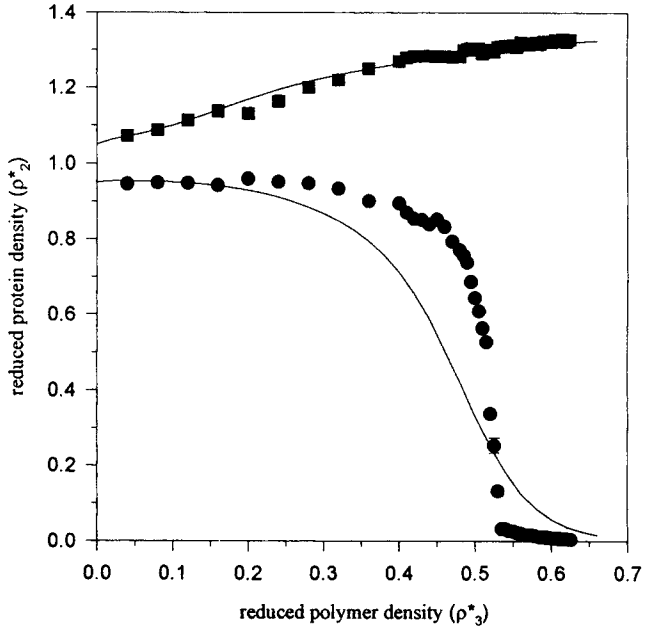

Figure 4. Phase diagram for the Asakura and Oosawa fluid with $d_3/d_2 = 0.20$.

The circles are the fluid and the squares are the solid coexistence densities obtained from the Gibbs–Duhem integration. The line corresponds to the results of second-order perturbation theory.

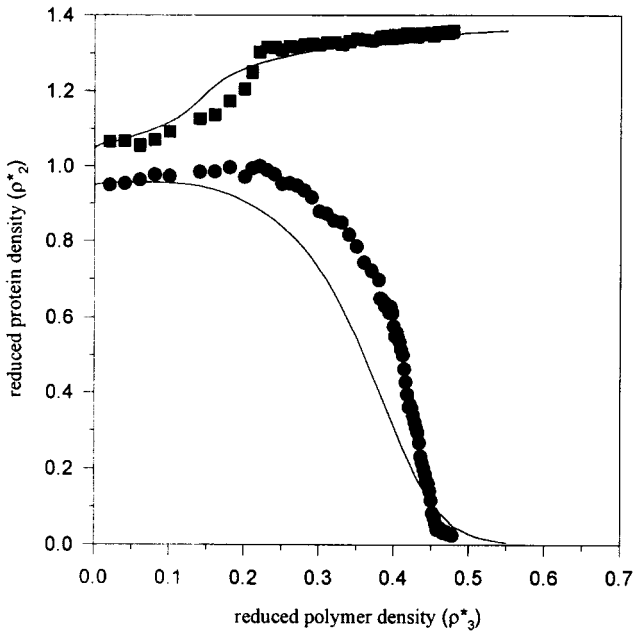

Figure 5. Phase diagram for the Asakura and Oosawa fluid for $d_3/d_2 = 0.14$.

The circles are the fluid and the squares are the solid coexistence densities obtained from the Gibbs–Duhem integration. The line corresponds to the results of second-order perturbation theory.

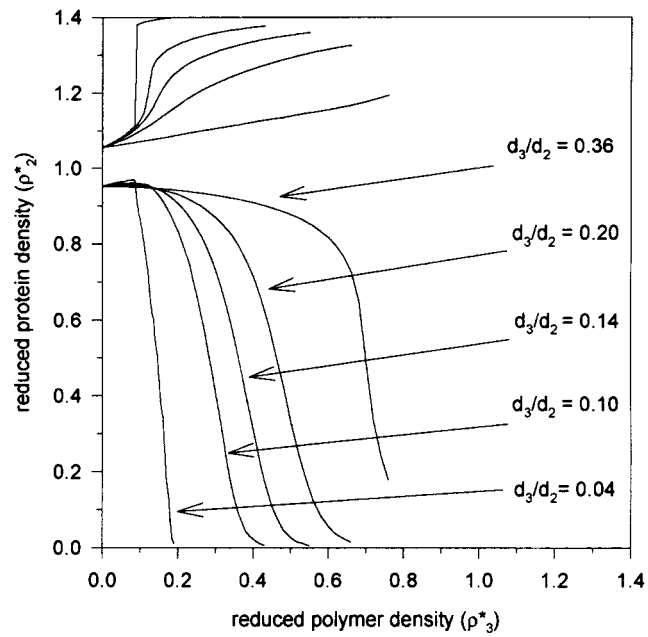

Figure 6. Fluid–solid coexistence lines for the Asakura and Oosawa fluid for $d_3/d_2 = < 0.40$ obtained from second-order perturbation theory.

symbols designating the solid and fluid phases, respectively, for these parameter values. The Gibbs-ensemble simulation shows that there is no stable fluid–fluid phase transition. This suggests that for this range of conditions the protein crystallizes rather than precipitating as an amorphous, high-density phase. Second-order Baker and Henderson perturbation theory predicts, at least qualitatively, the behavior obtained in the simulations. The results from perturbation theory indicate that for a relative polymer diameter (d_3/d_2) larger than 0.4, the system has stable liquid–liquid and solid–liquid transitions, as shown for $d_3/d_2 = 1.0$ in Figure 3. In this case the fluid has both liquid–liquid critical and triple points. However, for d_3/d_2 smaller than 0.4, the Asakura and Oosawa potential allows only a solid–fluid transition, and no stable liquid–liquid transition or critical point appears. Phase diagrams for the Asakura and Oosawa fluid for $d_3/d_2 < 0.40$ obtained from perturbation theory are shown in Figure 6. As d_3/d_2 decreases, the attractive effect and the short-range character of the Asakura–Oosawa potential increases. As a result, a lower concentration of polymer (in terms of ρ_3^*) is required to induce phase separation (protein precipitation). Also for the case of d_3/d_2 equal to 0.04, the system has an isostructural (FCC) first-order solid–solid transition. Similar results were observed by Bolhuis and Frenkel (1994), Bolhuis et al. (1994), and Frenkel et al. (1996) when studying the square-well and Yukawa fluids when a very short-ranged attractive part was used. Figure 7 shows the results for the vapor–liquid coexistence and critical points of the Asakura and Oosawa potential for different values of d_3/d_2 obtained from the perturbation theory. For d_3/d_2 equal to 0.20 and 0.40, the perturbation theory shows that the vapor–liquid lines are not stable. The critical points, indicated by the points on the coexistence lines exhibit a maximum as a function of ρ_3^*, but increase systematically with ρ_2^* (see also Figure 11, discussed later).

The results presented here are consistent with those of Gast et al. (1983a) and Mahadevan and Hall (1990), who have used Baker–Henderson (1967) perturbation theory with the macroscopic compressibility approximation for the second-

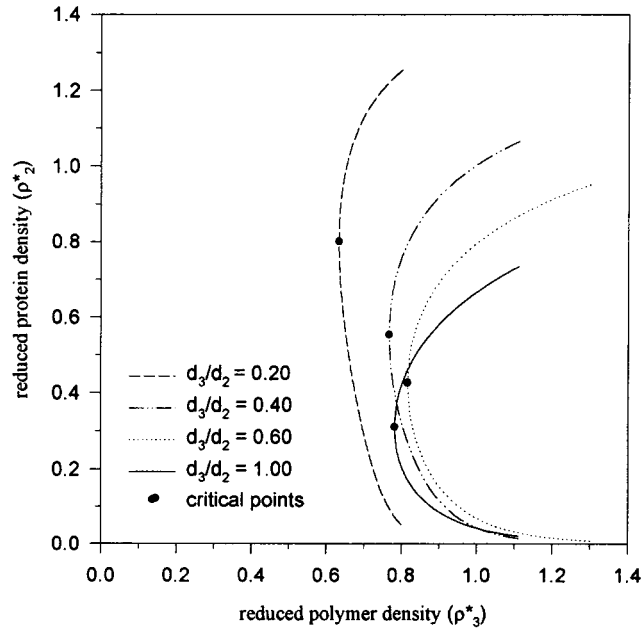

Figure 7. Liquid–liquid coexistence and critical points for the Asakura and Oosawa fluid for different values of d_3/d_2 obtained from second-order perturbation theory.

order term. Our results are also consistent with those for the phase diagram for the hard-core attractive Yukawa fluid of Hagen and Frenkel (1994). These authors have shown that for sufficiently short-range interactions, the vapor–liquid critical point disappears and only the solid–fluid coexistence curve is thermodynamically stable. In contrast, for a long-range attraction, the system can exist as a vapor, liquid, or solid, and both vapor–liquid and solid–liquid coexistence curves are present.

By using NVT-ensemble simulations to calculate the perturbation contributions for the fluid and solid phases, Hagen and Frenkel (1994) have shown that first-order perturbation theory works reasonably well and qualitatively predicts all the behavior observed from the Gibbs-ensemble simulation and the Gibbs–Duhem integration techniques. Because of the need for NVT-ensemble simulation results to compute the perturbation contributions in both phases, the perturbation theory calculations of Hagen and Frenkel are limited to the values of temperature, density, and potential parameters used by them. We have used analytic real function expressions for the RDF of the reference systems in both phases, which permits using the local compressibility approximation without any nonanalytic derivative terms, thereby speeding up phase-equilibrium calculations.

In order to study the effect of electrostatic forces (the charge–charge contribution) and the van der Waals interaction to the protein–protein potential, we have also calculated the isothermal ($T^* = 1.0$) phase diagram for this more complete potential using second-order perturbation theory. To incorporate these contributions, the perturbation part of the effective potential is given directly by the full potential, $u_p^* = u_R^* + u_A^* + u_{OA}^*$, each part of which is given in Eqs. 2 to 7. Figures 8 and 9 show the calculated phase diagrams for relative polymer diameters of $d_3/d_2 = 0.20$ and 0.10, respectively. In these calculations, we have fixed the nondimensional Debye screening length at $k^* = 8.0$ and the Hamaker constant at $H^* = 10.0$, and compared the results with those obtained using only the Asakura–Oosawa potential. The parameter A^*, directly related to the charge of the protein (or to the pH of the solution), was changed from 0 to 20. For fixed values

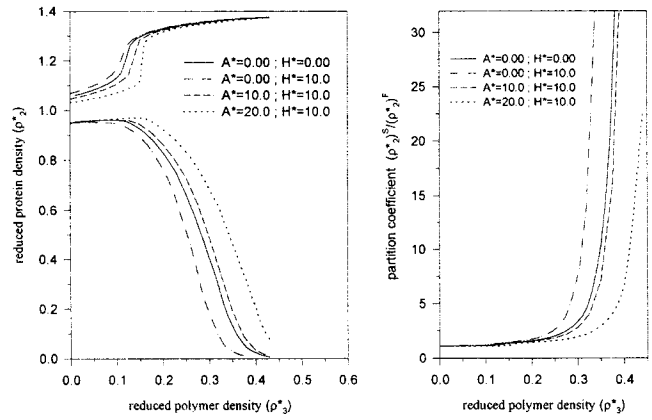

Figure 9. Fluid–solid coexistence (a) and partition coefficient (b) curves for the complete protein potential for different values of the protein charge (or pH of the solution) obtained from second-order perturbation theory ($d_3/d_2 = 0.10$ and $k^* = 8.0$).

of H^*, A^*, d_3/d_2, Figure 10 shows how the phase diagram changes for different values of the Debye screening length (which is directly related to the ionic strength of the solution). Figure 11 presents the vapor–liquid critical points calculated from the perturbation theory of the overall protein potential for different values of d_3/d_2. As shown in the figures, the shape of the phase diagram is not very sensitive to the value of the parameter A^* or k^*; which is expected since the attractive short-range character of the potential does not change for the different values of A^* (or k^*) studied here. Although the electrostatic effect does not change the general shape of the phase diagram, it plays an important quantitative role in polymer-induced protein precipitation. This can be seen by looking at the values of the partition coefficient (Figures 8, 9, and 10), defined as the ratio of protein densities in the two phases (ρ_2^{*S}/ρ_2^{*F}). This partition coefficient is sensitive to the values of the potential parameters A^*, H^*, d_3/d_2, and k^*. For a fixed polymer diameter, Figures 8 and 9 show that the

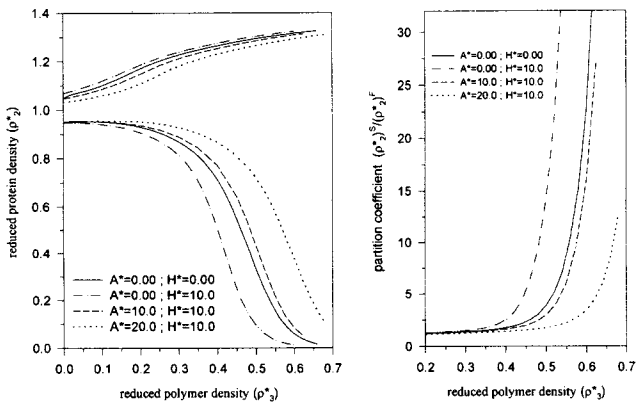

Figure 8. Fluid–solid coexistence (a) and partition coefficient (b) curves for the complete protein potential for different values of the protein charge (or pH of the solution) obtained from second-order perturbation theory ($d_3/d_2 = 0.20$ and $k^* = 8.0$).

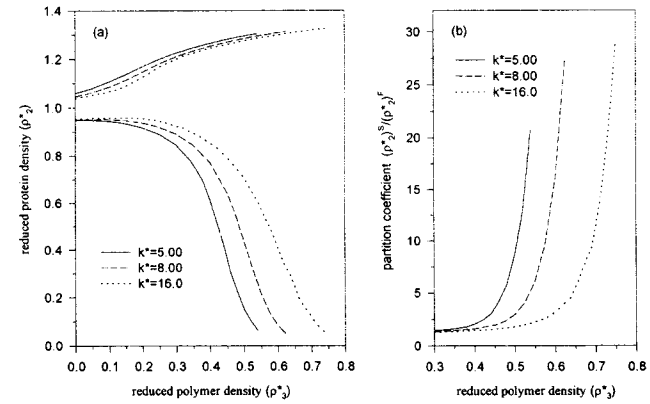

Figure 10. Fluid–solid coexistence curves (a) and partition coefficients (b) for different values of the ionic strength of the solution obtained from second-order perturbation theory ($d_3/d_2 = 0.20$, $A^* = 10.0$, and $H^* = 10.0$).

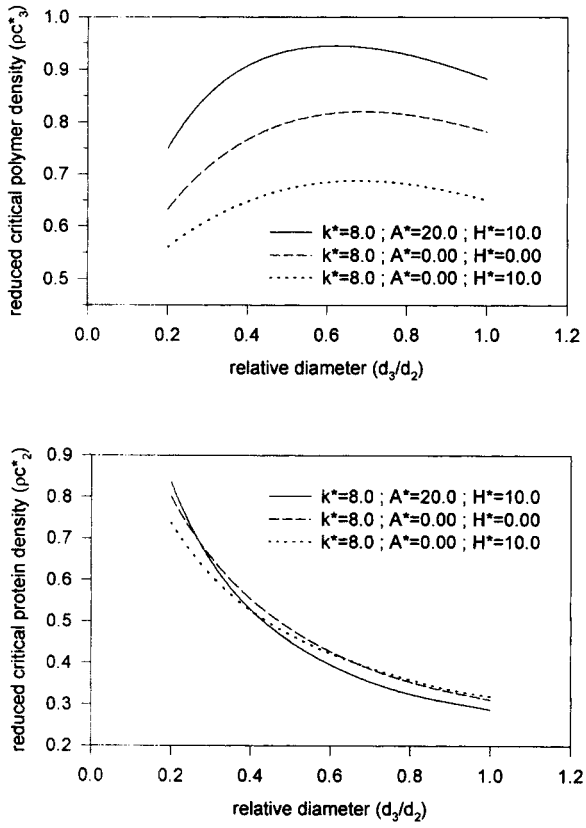

Figure 11. Liquid–liquid critical points calculated from second-order perturbation theory for the complete protein potential for different values of the ratio d_3/d_2.

partition coefficient increases with increasing protein diameter when other parameters are kept constant. Also, in agreement with experimental data, larger proteins precipitate out at lower PEG concentrations than smaller proteins. Also we see from these figures that the partition coefficient decreases as A^* increases. As expected, by decreasing the electrostatic repulsion at a fixed value of ionic strength, the relative contribution of the attractive potential increases producing a decrease of solubility. A similar effect is observed when decreasing the value of ionic strength, while A^* and other parameters are kept constant (Figure 10). All of these results are consistent with the experimental observations reported by Atha and Ingham (1981) that the protein solubility decreases as the pH approaches the isoelectric point (A^* decreases) or as the ionic strength is increased (k^* increases). In addition, these figures show the influence of dispersion interaction; a higher value of the Hamaker constant yields a higher value of the partition coefficient. However, since the potential of the mean-force model that we have used is a simple one, we have not attempted to fit experimental data.

Conclusions

We have used the one-component potential of mean-force approximation to describe protein–protein interactions and to calculate the precipitation of proteins induced by polymers. The effective protein–protein interaction in the presence of the polymer is mainly related to the Asakura–Oosawa potential, but the effects of the protein charge, pH of the solution, ionic strength of the solution, and van der Waals attraction are also included in the potential. Although the potential model used here does not account for other, more complicated forces that are known to be important, such as the direct salt effect, the protein–protein association, and nonpairwise additivity, at least for some conditions and protein solutions, the simple potential model used here with either simulation methods or perturbation theory is able to predict the general trends observed experimentally in protein precipitation.

In order to establish a rational basis to improve our understanding of intermolecular forces and to better model protein systems, it is useful to test the validity of the computational approximations for a specified potential of mean force. Here we have combined the Gibbs-ensemble Monte Carlo simulation to calculate the fluid–fluid phase transition and the Gibbs–Duhem integration to calculate the solid–fluid phase coexistence behavior for the Asakura–Oosawa fluid. We have also used second-order Barker and Henderson perturbation theory to compute the phase diagrams for protein solutions modeled by both the Asakura–Oosawa potential and the more complete potential considered here that accounts for the volume-exclusion effect (Asakura–Oosawa), the charge on the polyion (or pH of the solution), the ionic strength of the solution, and the van der Waals interactions. We have shown that this perturbation theory is able to predict the general phase behavior observed from the simulation methods. In particular, both simulation and perturbation theory show that the system modeled by this potential of mean force has a fluid–fluid critical point that disappears when the potential becomes too short range.

Comparing the phase diagram predicted by perturbation theory with the simulation data, we see that second-order Barker and Henderson perturbation theory with the local compressibility approximation is reasonably accurate for the calculation of phase equilibria for the potential used here. The use of analytic real functions to evaluate the RDF for the hard-sphere reference systems in both solid and fluid phases permits using the local compressibility approximation without any nonanalytic differential terms, and also speeds up the phase-equilibrium calculations. This perturbation theory has the advantages of being sufficiently simple and reasonably accurate for engineering use.

Perhaps, most importantly, we have used both simulation and perturbation theory to establish that polymer-induced protein deposition can be by either crystallization or precipitation as a dense amorphous phase, and that such behavior can be predicted on a fundamental basis. Consequently, the methods used here can form the basis for predicting whether crystallization or amorphous precipitation will occur, and how the boundary between these two forms of deposition changes with changes in solution conditions

Acknowledgments

The first author (F. W. T.) gratefully acknowledges the financial support of the CNPq/Brazil (Conselho Nacional de Desenvolvimento Científico e Tecnológico). The preparation of this manuscript was supported in part by grant DE-FG02-85ER13436 from the U.S. Department of Energy, and in part by grant BES-9210401 from the

U.S. National Science Foundation, both to the University of Delaware. We thank J. Chang, J. Bergenholtz, and N. J. Wagner (University of Delaware), D. Kuehner, W. Blanch, and J. M. Prausnitz (University of California–Berkeley), and D. A. Kofke (State University of New York at Buffalo) for their suggestions and useful comments.

Notation

A^* = nondimensional parameter of the screened Coulomb potential defined by Eq. 3
e = elementary charge, 1.602×10^{-19} C
e^* = reduced configurational energy
I_i = integral contributions that appear in the first ($i = 1$) and second ($i = 2$) orders in perturbation theory
k = inverse of the Debye screening length
P^* = reduced pressure
r = interprotein center-to-center distance
v = molar volumes
z = valence of the polyion
ϵ_0 = permittivity in vacuum
* = nondimensional variables

Literature Cited

Agrawal, R., and D. A. Kofke, "Thermodynamic and Structural Properties of Model Systems at Solid-Fluid Coexistence I. FCC and BCC Soft Sphere," *Mol. Phys.*, **85**, 23 (1995a).

Agrawal, R., and D. A. Kofke, "Thermodynamic and Structural Properties of Model Systems at Solid-Fluid Coexistence II. Melting and Sublimation of the Lennard-Jones System," *Mol. Phys.*, **85**, 43 (1995b).

Allen, M. P., and D. J. Tildesley, *Computer Simulation of Liquids*, Clarendon Press, Oxford (1987).

Asakura, S., and F. Oosawa, "On Interaction Between Two Bodies Immersed in a Solution of Macromolecules," *J. Chem. Phys.*, **22**, 1255 (1954).

Asakura, S., and F. Oosawa, "Interaction Between Particles Suspended in Solutions of Macromolecules," *J. Poly. Sci.*, **33**, 183 (1958).

Atha, D. H., and K. C. Ingham, "Mechanism of Precipitation of Protein by Polyethylene Glycols," *J. Biol. Chem.*, **256**, 12108 (1981).

Barker, J. A., and D. Henderson, "Perturbation Theory and Equation of State for Fluids I: The Square-Well Potential," *J. Chem. Phys.*, **47**, 2856 (1967).

Bolhuis, P., and D. Frenkel, "Prediction of an Expanded-to-Condensed Transition in Colloidal Crystals," *Phys. Rev. Lett.*, **14**, 2211 (1994).

Bolhuis, P., M. Hagen, and D. Frenkel, "Isostructural Solid-Solid Transition in Crystalline Systems with Short-Ranged Interaction," *Phys. Rev. E*, **50**, 4480 (1994).

Boublik, T., I. Nezbeda, and K. Hlavaty, *Statistical Thermodynamics of Simple Liquids and their Mixtures*, Elsevier, New York (1980).

Carnahan, N. F., and K. E. Starling, "Equation of State for Nonattracting Rigid Spheres," *J. Chem. Phys.*, **51**, 635 (1969).

Chang, J., and S. I. Sandler, "A Real Function Representation for the Structure of the Hard-Sphere Fluid," *Mol. Phys.*, **81**, 735 (1994a).

Chang, J., and S. I. Sandler, "A Completely Analytic Perturbation Theory for the Square-Well Fluid of Variable Well Width," *Mol. Phys.*, **81**, 745 (1994b).

Chiew, Y. C., D. E. Kuehner, H. W. Blanch, and J. M. Prausnitz, "Molecular Thermodynamics for Salt-Induced Protein Precipitation," *AIChE J.*, **41**, 2150 (1995).

Coen, C. J., H. W. Blanch, and J. M. Prausnitz, "Salting Out of Aqueous Proteins: Phase Equilibria and Intermolecular Potentials," *AIChE J.*, **41**, 996 (1995).

De Hek, H., and A. Vrij, "Interactions in Mixtures of Colloidal Silica Spheres and Polystyrene Molecules in Cyclohexane," *J. Colloid Interf. Sci.*, **84**, 409 (1981).

Edmond, E., and A. G. Ogston, "An Approach to the Study of Phase Separation in Ternary Aqueous Systems," *Biochem. J.*, **109**, 569 (1968).

Forciniti, D. C., C. K. Hall, and M. R. Kula, "Protein Partitioning at the Isoelectric Point: Influence of Polymer Molecular Weight and Concentration and Protein Size," *Biotechnol. & Bioeng.*, **38**, 986 (1991).

Frenkel, D., P. Bladon, P. Bolhuis, and M. Hagen, "Liquid-Like Behavior in Solids," *Mol. Simulation*, **16**, 127 (1996).

Gast, A. P., C. K. Hall, and W. G. Russel, "Polymer-Induced Phase Separations in Nonaqueous Colloidal Suspensions," *J. Colloid Interf. Sci.*, **96**, 251 (1983a).

Gast, A. P., C. K. Hall, and W. G. Russel, "Phase Separations Induced in Aqueous Colloidal Suspensions by Dissolved Polymer," *J. Farad. Discuss. Chem. Soc.*, **76**, 189 (1983b).

Grimson, M. J., "Small-Angle Scattering from Colloidal Dispersion," *J. Chem. Soc. Farad. Trans.*, **79**(2), 817 (1983).

Hagen, M. H. J., and D. Frenkel, "Determination of Phase Diagrams for the Hard-Core Attractive Yukawa System," *J. Chem. Phys.*, **101**, 4093 (1994).

Haire, R. N., W. A. Tisel, J. G. White, and A. Rosenberg, "On the Precipitation of Proteins by Polymers: The Hemoglobin-Polyethylene Glycol System," *Biopolymers*, **23**, 2761 (1984).

Hall, K. R., "Another Hard-Sphere Equation of State," *J. Chem. Phys.*, **57**, 2252 (1971).

Haynes, C. A., K. Tamura, H. R. Korfer, H. W. Blanch, and J. M. Prausnitz, "Thermodynamic Properties of Aqueous α-Chymotrypsin Solutions from Membrane Osmometry Measurements," *J. Phys. Chem.*, **96**, 905 (1992).

Haynes, C. A., F. J. Benitez, H. W. Blanch, and J. M. Prausnitz, "Application of Integral-Equation Theory to Aqueous Two-Phase Partitioning System," *AIChE J.*, **39**, 1539 (1993).

Hoover, W. G., and F. H. Ree, "Melting Transition and Communal Entropy for Hard Sphere," *J. Chem. Phys.*, **49**, 3609 (1968).

Joanny, J. F., L. Leibler, and P. G. de Gennes, "Effects of Polymer Solutions on Colloid Stability," *J. Poly. Sci. Poly. Phys. Edition*, **17**, 1073 (1979).

Kincaid, J. M., and J. J. Weis, "Radial Distribution Function of a Hard-Sphere Solid," *Mol. Phys.*, **34**, 931 (1977).

Kofke, D. A., "Gibbs-Duhem Integration: A New Method for Direct Evaluation of Phase Coexistence by Molecular Simulation," *Mol. Phys.*, **78**, 1331 (1993a).

Kofke, D. A., "Direct Evaluation of Phase Coexistence by Molecular Simulation Via Integration Along the Saturation Line," *J. Chem. Phys.*, **89**, 4149 (1993b).

Kuehner, D. E., H. W. Blanch, and J. M. Prausnitz, "Salt-Induced Protein Precipitation: Phase Equilibria from an Equation of State," Fluid Phase Equilibria Meeting, Snowmass/Aspen, CO (1995).

Lekkerkerker, H. N. W., W. C.-K. Poon, and P. N. Pusey, "Phase Behavior of Colloid + Polymer Mixtures," *Europhys. Lett.*, **20**, 559 (1992).

Mahadevan, H., and C. K. Hall, "Statistical-Mechanical Model of Protein Precipitation by Nonionic Polymer," *AIChE J.*, **36**, 1517 (1990).

Mahadevan, H., and C. K. Hall, "Theory of Precipitation of Protein Mixtures by Nonionic Polymer," *AIChE J.*, **38**, 573 (1992).

McQuarrie, D. A., *Statistical Mechanics*, Harper-Collins, New York (1976).

Panagiotopoulos, A. Z., "Direct Determination of Phase Coexistence Properties of Fluids by Monte Carlo Simulation in a New Ensemble," *Mol. Phys.*, **61**, 813 (1987).

Panagiotopoulos, A. Z., N. Quirke, M. Stapleton, and D. J. Tildesley, "Phase Equilibria by Simulation in the Gibbs Ensemble: Alternative Derivation, Generalization and Application to Mixture and Membrane Equilibria," *Mol. Phys.*, **63**, 527 (1988).

Panagiotopoulos, A. Z., "The Gibbs Method for Calculating Phase Equilibria by Simulation," *Mol. Simulation*, **9**, 1 (1992).

Panagiotopoulos, A. Z., "Molecular Simulation of Phase Equilibria," *Supercritical Fluids-Fundamentals for Application*, E. Kiran and J. M. H. L. Senger, eds., Kluwer, Dordrecht, The Netherlands, p. 411 (1994).

Press, W. H., S. A. Teukolsky, W. T. Vetterling, and B. P. Flannery, *Numerical Recipes in FORTRAN: The Art of Scientific Computing*, Cambridge Univ. Press, Cambridge, England (1992).

Recht, J. R., and A. Z. Panagiotopoulos, "Finite-Size Effects and Approach to Criticality in Gibbs Ensemble Simulations," *Mol. Phys.*, **80**, 843 (1993).

Smit, B., *Simulation of Phase Coexistence: From Atoms to Surfactants*, PhD thesis, Rijksuniversiteit Utrecht, The Netherlands (1990).

Smit, B., and D. Frenkel, "Vapour-Liquid Equilibria of the Hard Core Yukawa Fluid," *Mol. Phys.*, **74**, 35 (1991a).
Smit, B., and D. Frenkel, "Vapour-Liquid Equilibria of the Two-Dimensional Lennard-Jones Fluid," *J. Chem. Phys.*, **94**, 5663 (1991b).
Shih, Y.-C., H. W. Blanch, and J. M. Prausnitz, "Some Characteristics of Protein Precipitation by Salts," *Biotechnol & Bioeng.*, **40**, 1155 (1992).
Sperry, P. R., H. B. Hopfenberg, and N. L. Thomas, "Flocculation of Latex by Water-Soluble Polymers: Experimental Confirmation of a Nonbridging, Nonadsorptive, Volume-Restriction Mechanism," *J. Colloid Interf. Sci.*, **82**, 62 (1981).
Tavares, F. W., and S. I. Sandler, "Vapour-Liquid Equilibria of Exponential-Six Fluids," *Mol. Phys.*, **87**, 1471 (1996).
Verwey, E. J. W., and J. T. K. Overbeek, *Theory of Stability of Lyophobic Colloids*, Elsevier, Amsterdam (1948).
Victor, J. M., and J. P. Hansen, "Liquid-Gas Transition in Charged Colloidal Dispersions," *J. Phys. Lett.*, **45**, L-307 (1984).
Vilker, V. L., C. K. Colton, and K. A. Smith, "The Osmotic Pressure of Concentrated Protein Solutions: The Effect of Concentration and pH in Saline Solutions of Bovine Serum Albumin," *J. Colloid Interf. Sci.*, **79**, 548 (1981).
Vincent, B., P. F. Lucham, and F. A. Waite, "The Effect of Free Polymer on the Stability of Sterically Stabilized Dispersions," *J. Colloid Interf. Sci.*, **73**, 508 (1980).
Vlachy, V., and J. M. Prausnitz, "Donnan Equilibrium. Hypernetted-Chain Study of One- and Multicomponent Model for Aqueous Polyelectrolyte Solutions," *J. Phys. Chem.*, **96**, 6465 (1992).
Vlachy, V., H. W. Blanch, and J. M. Prausnitz, "Liquid-Liquid Phase Separation in Aqueous Solutions of Globular Proteins," *AIChE J.*, **39**, 215 (1993).
Vrij, A., "Polymer at Interfaces and the Interactions in Colloidal Dispersions," *Pure and Appl. Chem.*, **48**, 471 (1976).
Yeomans, J. M., *Statistical Mechanics of Phase Transitions*, Oxford Univ. Press, New York (1992).

Manuscript received Mar. 25, 1996, and revision received Aug. 5, 1996.